

Spatio-temporal exploratory analysis of urban surface temperature field in Shanghai, China

Xiaoyan Dai · Zhongyang Guo · Liquan Zhang · Dan Li

Published online: 8 July 2009
© Springer-Verlag 2009

Abstract The integrated application of remote sensing, geographic information system and quantitative analytical modeling can provide scientific and effective methods for monitoring and studying urban heat island, based on land surface temperature (LST) retrieved from thermal infrared channel data of sensors. In this paper, LST is retrieved from Landsat TM6 and ETM + 6 data of Shanghai central city in 1989, 1997, 2000 and 2002, by using the mono-window algorithm. Based on the data, global and local spatial autocorrelation analysis, and geostatistical methods are adopted to quantitatively describe the characteristics of spatial heterogeneity and temporal evolution of land surface thermal landscape at different scales and periods in Shanghai central city, by utilizing exploratory spatial data analysis. Results show that LST field in Shanghai central city tends to fragmentize and complicate with the development of Shanghai, and its global spatial difference becomes greater gradually. The spatial variance pattern of the change of LST field from 1997 to 2002 indicates that

the dynamic change of LST presents a tendency of increase in circularity. LST declines distinctly in the districts of Puxi and Pudong near and inside the inner ring road, while it rises obviously outside the central city and near the out ring road. The extrema of temporal change in LST field have a characteristic of spatial clustering. Besides, as the city of Shanghai expands in a circular pattern as a whole, the directional difference of dynamic change of urban surface thermal landscape exists but is not very obvious.

Keywords Land surface temperature · Urban heat island · Exploratory spatial data analysis · Shanghai

1 Introduction

Land surface temperature (LST) is a key factor in physical processing of land surface at a regional and a global scale, and it generalizes the results of the interaction between land surface and atmosphere, and the exchange of matter and energy (Wan and Dozier 1996). Moreover, in the general assessment model of sustainable development and global change, the change of LST is regarded as an important criterion upon which the evaluation of environmental quality and social and economic development policy can be based (Janssen 1998; Tamerius et al. 2007; Keller 2008).

Traditional in situ ground measurements can provide comparatively accurate LST value, while they cannot reveal the change of land surface thermal environment comprehensively and synchronously, due to the limited spatio-temporal extension of in situ measurements and great demands for manpower and financial resources. On the other hand, remote sensing data have the advantages of wide scope, periodical overlap, and comparative low-cost.

X. Dai · L. Zhang
State Key Laboratory of Estuarine and Coastal Research,
East China Normal University, 200062 Shanghai,
People's Republic of China
e-mail: dxiaoyan2002@yahoo.com.cn

Z. Guo (✉)
Department of Geography, Key Laboratory of Geographic
Information Science, Ministry of Education, East China Normal
University, 200062 Shanghai, People's Republic of China
e-mail: zyguo@geo.ecnu.edu.cn

D. Li
School of Electrical Engineering and Information, Anhui
University of Technology, 243002 Ma'anshan,
People's Republic of China

As the study on LST retrieval from remote sensing data proceeds deeper and the accuracy of LST retrieval increases gradually, nowadays, LST retrieval from thermal infrared band data of remote sensors has become one of the major approaches to obtain information about LST spatio-temporal distribution (Gallo et al. 1995; Owen et al. 1998). The integrated application of remote sensing, geographic information system (GIS) and quantitative analytical modeling can provide scientific and effective methods for monitoring and studying urban land surface thermal environment. Chen et al. (2002) utilized the fractal tool to reveal the whole, regional and microcosmic characteristics of urban thermal environment, and developed three fractal dimension measurement methods to analyze the fractal characteristics of the whole thermal field in the city of Shanghai, China, the thermal structure of its typical regions and gradient of the thermal field distribution. Xu and Chen (2003) normalized and graded two LST images acquired in June, 1989 and April, 2000, and devised an urban heat island ratio index (URI) to quantitatively study urban heat island (UHI) changes during the study period, and reduce the influence of seasonal difference on the dynamical change of UHI to a certain extent. Streutker (2002) and Zhang et al. (2007) respectively adopted a Gaussian-based density slice method and a robust statistical method to divide the LST data of different years and seasons into several LST levels for an exploration of the spatio-temporal change of LST field distribution in the study area. Tran et al. (2006) applied a 2-D Gaussian surface approximation to quantify spatial extents and magnitude of individual UHIs for a comparative assessment of the UHI spatial patterns and temporal variation in eight Asian mega cities in both temperate and tropical climate regions from 2001 to 2003.

Spatial statistical method is used to reveal the spatial dependence, spatial association and spatial autocorrelation among spatial data by adopting various spatial statistical analytic models. As a core technique in spatial statistical analysis, exploratory spatial data analysis (ESDA) technique can be applied to study spatial dependence and heterogeneity by analyzing spatial autocorrelation, and reveal the characteristics of spatial data, detect singular points or regions, explore spatial association pattern, clustering or hot-spot, and make spatial partition by means of visualization tools (Anselin 1999; Ma et al. 2002; Morakinyo and Mackay 2005; Olea 2006; Brenning and Dubois 2008). To explore the spatio-temporal evolution of urban thermal environment during the rapid social and economic development of Shanghai, in this paper, LST is retrieved from Landsat 5 Thematic Mapper (TM) and Landsat 7 Enhanced Thematic Mapper Plus (ETM+) thermal channel data covering Shanghai central city in 1989, 1997, 2000 and 2002, by using mono-window algorithm. Based on the

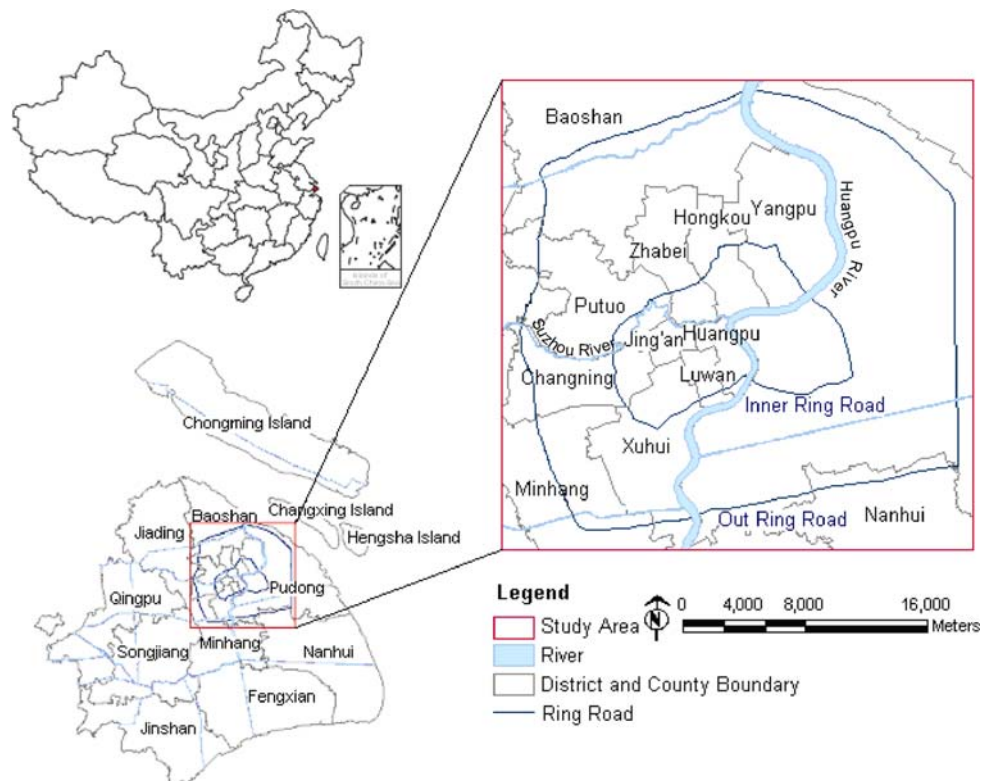
data, global and local spatial autocorrelation analysis and geostatistical methods are adopted to reveal the characteristics of spatial heterogeneity and temporal evolution of land surface thermal landscape at different scales and periods in Shanghai central city with ESDA. In Sect. 2 we describe the data sources, and the preprocess to rectify remote sensing images and other vector thematic maps and retrieve LST from Landsat TM6 and ETM + 6 data. The description of spatial distribution of LST field is presented in Sect. 3. In Sect. 4 we describe the characteristics of spatial heterogeneity and temporal evolution of land surface thermal landscape at different scales and periods with ESDA. The last section summarizes our main conclusions.

2 Data and preprocessing

Shanghai lies between 30°23′–31°37′N and 120°50′–121°45′E, belonging to the alluvial plain of Yangtze River Delta, to the west of the Yangtze River estuary, with a total area of approximately 8,239 km² covering eighteen districts and one county. With a pleasant subtropical maritime monsoon climate, Shanghai has a temperate climate, plenty of rainfall and four distinct seasons, with an annual average temperature of 15–16°C and annual average precipitation amount of about 1,100 mm. Preferable geographical location and natural condition provide favorable natural basis upon which the exploitation and utilization of land resources and rapid social and economic development of Shanghai rest. However, since the reform and opening of Shanghai progress at an unprecedented pace, Shanghai has experienced a notable change of land use structure, and a series of urban ecological environmental problems, such as soil, water and atmosphere pollution, UHI, and so on.

Shanghai was at the peak of urban renewal and the stage of large-scale development of the whole Pudong area from 1992 to 2002. The course of urban renewal has witnessed a rapid spatial sprawl of urban land, and the developed area of the city is located mainly inside the outer ring road. To explore the UHI effect accompanied by the change of urban landscape layout and land use pattern during this period, in this paper, Landsat 5 TM image acquired on Aug 11, 1989, Landsat 7 ETM + images acquired on Apr 11, 1997, June 14, 2000 and Nov 11, 2002 are used as primary data source. The study area includes Shanghai central city inside the out ring road, and meanwhile, partial suburban areas near the out ring road for a contrast between city and suburbs (Fig. 1). The images of bands 1–7 are geometrically rectified to 1:10000 vector topographic map with Gauss-Krueger projection, and resampled by adopting the nearest-neighbor algorithm with a pixel size of 30 m by 30 m for bands 1–5 and 7, 60 m by 60 m for ETM + 6, and 120 m by 120 m for TM6. The resultant root mean

Fig. 1 Map of the study area



square error (RMSE) of the corrected images is found to be less than half a pixel. In addition, the remote sensing images and other vector thematic maps used for auxiliary analysis, such as land use classification images, population, economy and traffic distribution images, and district maps, etc., are all rectified to a Shanghai local coordinate system.

Before LST retrieval, the brightness temperature of the thermal band at the satellite level must be computed from the ETM + 6 and TM6 data. The computation of brightness temperature involves the estimation of spectral radiance from digital numbers (DNs) of band 6 using the following Eqs. 1 and 2, and the conversion of the radiance into brightness temperature using the Eq. 3 (Wukelic et al. 1989; Chander and Markham 2003).

$$L_{\lambda} = L_{\min_{\lambda}} + \frac{L_{\max_{\lambda}} - L_{\min_{\lambda}}}{255} \times \text{DN} \quad (1)$$

$$L_{\lambda} = \text{gain} \times \text{DN} + \text{offset} \quad (2)$$

where L_{λ} is the spectral radiance received by the sensor ($\text{W m}^{-2} \text{sr}^{-1} \mu\text{m}^{-1}$), $L_{\max_{\lambda}}$ and $L_{\min_{\lambda}}$ are the maximum and minimum detected spectral radiance for $\text{DN} = 255$ and $\text{DN} = 0$, respectively, and gain and offset are rescaled gain and bias value supplied in the Level 1G Landsat 7 ETM + image header or ancillary data record both in $\text{W m}^{-2} \text{sr}^{-1} \mu\text{m}^{-1}$. For TM6 of Landsat 5, it has been set that $L_{\min_{\lambda}} = 1.238 \text{ W m}^{-2} \text{sr}^{-1} \mu\text{m}^{-1}$ for $\text{DN} = 0$ and $L_{\max_{\lambda}} = 15.6 \text{ W m}^{-2} \text{sr}^{-1} \mu\text{m}^{-1}$ for $\text{DN} = 255$.

$$T_6 = \frac{K_2}{\ln(1 + K_1/L_{\lambda})} \quad (3)$$

where T_6 is the effective at-satellite brightness temperature in K, K_1 and K_2 are pre-launch calibration constants. For Landsat 5, $K_1 = 607.76 \text{ W m}^{-2} \text{sr}^{-1} \mu\text{m}^{-1}$ and $K_2 = 1260.56 \text{ K}$, and for Landsat 7, $K_1 = 666.09 \text{ W m}^{-2} \text{sr}^{-1} \mu\text{m}^{-1}$ and $K_2 = 1282.71 \text{ K}$, respectively.

Based on the above, LST is retrieved from the ETM + 6 and TM6 data by using mono-window algorithm (Qin et al. 2001). The derivation of the mono-window algorithm considering the influence of atmospheric and land surface condition on land surface heat exchange is based on the thermal radiance transfer equation and needs three parameters including emissivity, atmospheric transmittance and effective mean atmospheric temperature. Comprehensive assessment indicates that the algorithm is able to provide accurate LST retrieved from Landsat thermal band data, and for the estimate of the essential parameters with moderate errors, the probable LST estimation error is less than 1.1°C (Qin et al. 2001). The results of experiments in different test areas indicate that the accuracy of the algorithm is satisfactory (Zhang et al. 2005; Huang et al. 2006; Ding and Xu 2006). Provided that the data set of land surface emissivity (LSE), atmospheric transmittance, and effective mean atmospheric temperature are available, the LST T_s , is obtained by the following equation:

$$T_s = \{67.3554(C + D - 1) + [0.4586 + 0.5414(C + D)]T_6 - DT_a\}/C \quad (4)$$

where T_6 is the at-satellite brightness temperature in K, T_a represents the effective mean atmospheric temperature in K, and C and D are given by the following equations:

$$C = \varepsilon_6 \tau_6 \quad (5)$$

$$D = (1 - \tau_6)[1 + (1 - \varepsilon_6)\tau_6] \quad (6)$$

where ε_6 is the emissivity, and τ_6 is the atmospheric transmittance.

According to the characteristics of land cover in the study area and spatial resolution of the utilized remote sensing images, for the purpose of dynamic monitoring, the land use in Shanghai central city is classified into five classes, namely, high albedo building (H), low albedo building (L), water (W), vegetation (V) and soil (S) by applying mixed-pixel classification based on a Possibilistic C Repulsive Medoids (PCRMdd) clustering algorithm (Dai et al. 2009). Each of the land use categories is assigned an emissivity value by reference to the emissivity classification scheme proposed by Snyder et al. (1998) and Qin et al. (2004). In this study, the emissivity value for high albedo building, low albedo building, water, vegetation and soil are set to 0.970, 0.962, 0.995, 0.985 and 0.976, respectively.

The two atmospheric parameters, T_a and τ_6 , required for the algorithm can be estimated according to local meteorological observation data, such as the near-surface air temperature and atmospheric water vapor content. In the standard atmospheric conditions, i.e., clear sky and without great turbulence, T_a can be estimated from T_0 , air temperature of the ground (at about 2 m height) for mid-latitude summer and winter by the linear relations (7) and (8), respectively, as follows:

Table 1 Estimation of atmospheric transmittance in the mono-window algorithm

Profiles	Water vapour (w) (g cm ⁻²)	Transmittance estimation equation
High air temperature	0.4–1.6	$\tau_6 = 0.974290 - 0.08007w$
	1.6–3.0	$\tau_6 = 1.031412 - 0.11536w$
Low air temperature	0.4–1.6	$\tau_6 = 0.982007 - 0.09611w$
	1.6–3.0	$\tau_6 = 1.053710 - 0.14142w$

$$T_a = 16.0110 + 0.92621 T_0 \quad (7)$$

$$T_a = 19.2704 + 0.91118 T_0 \quad (8)$$

Atmospheric transmittance τ_6 , can be estimated from w , the total atmospheric water vapour content, for the range 0.4–3.0 g/cm² by the equations shown in Table 1.

If the total atmospheric water vapour content is not available, τ_6 can be approximately estimated as

$$w = w(0)/R_w(0) \quad (9)$$

where $w(0)$ is water vapour content near the surface (at about 2 m height), which can be usually obtained from local meteorological data, and $R_w(0)$ is the ratio of atmospheric water vapour content near the surface to the total water vapour content which can be substituted with standard atmospheric ratio, i.e., 0.438446 and 0.400124 for mid-latitude summer and winter, respectively.

3 Spatial distribution of LST field

The distribution images of LST on Aug 11, 1989, Apr 11, 1997, June 14, 2000 and Nov 11, 2002 are acquired as shown in Fig. 2. To explore the spatial distribution of LST field during the study period and reduce the influence of

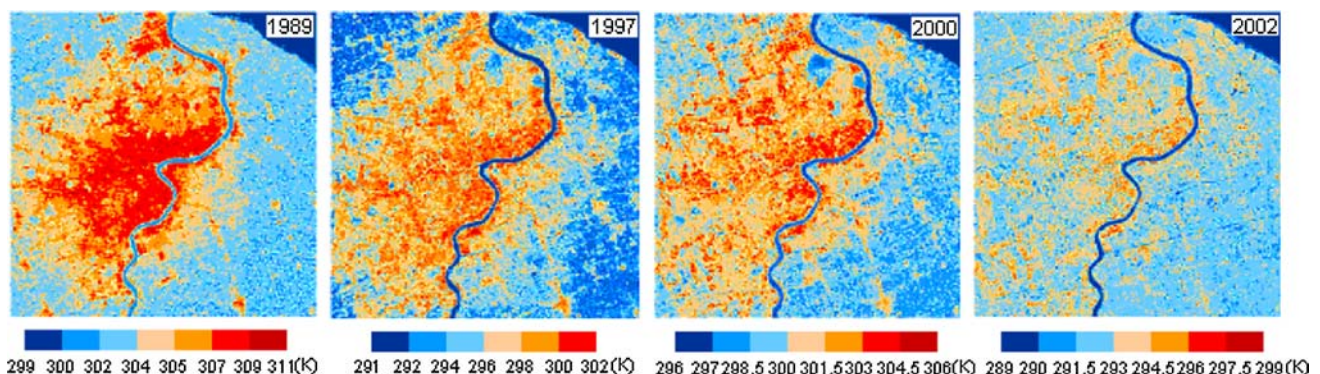
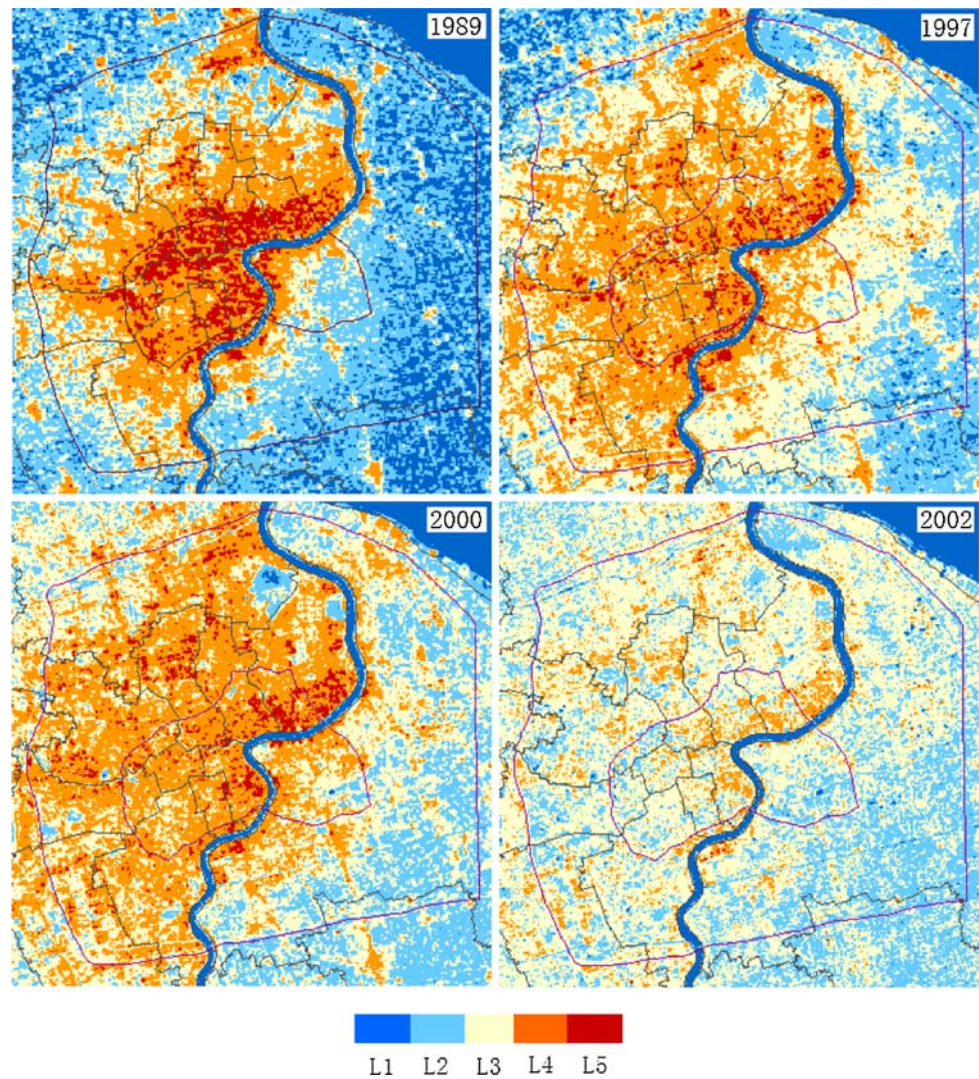


Fig. 2 LST distribution image in 1989, 1997, 2000 and 2002

Fig. 3 Distribution of LST levels in 1989, 1997, 2000 and 2002



seasonal difference on the study on LST dynamical change, the resultant multi-temporal LST images are divided into five levels, i.e., lower LST zone (L1), low LST zone (L2), medium LST zone (L3), high LST zone (L4) and thermal kernel zone (L5) by using density-based segmentation and unsupervised classification method (Fig. 3). Figure 3 represents the general pattern of LST spatial distribution in Shanghai central city. The boundary of high-temperature zone in the thermal field is consonant with the profile of the built-up area as a whole. The LST decreases gradually in circularity from the high temperature kernel in downtown to urban fringe, which forms obvious UHI effect. The high-speed social and economic development of Shanghai and the regulation of city spatial layout lead to notable changes in the distribution of population, buildings, traffic and industry in Shanghai central city, and accordingly, changes in the surface thermal landscape. Furthermore, it can be found from the evolution process of LST field pattern from 1989 to 2002 that, the area and intensity of Shanghai UHI

rapidly sprawls and strengthens from 1980s, and the expansion direction of UHI is consistent with that of urban area. However, since the end of the twentieth century, UHI effect shows a weakening tendency, and the difference in LST value inside the urban area minishes gradually. Until 2002, the high-temperature zone stops enlarging and the thermal kernel zone begins to diminish. Although on the whole, the LST in Pudong area is widely lower than that in Puxi area, the LST has an obvious increasing trend with the intensifying development of Pudong area along the Huangpu River since the opening up of Pudong New Area.

4 Spatio-temporal exploratory analysis of LST field

4.1 Global spatial autocorrelation analysis of LST field

Global spatial autocorrelation analysis can be used to describe the spatial characteristic of a given property in the

entire study area and reflect the mean of spatial difference between all the spatial cells and their adjacent cells. In this paper, the Global Moran's I statistic is used to measure the global spatial autocorrelation of the LST field and it can be calculated as (Goodchild 1986):

$$I = \frac{N}{S_0} \times \frac{\sum_{i=1}^N \sum_{j=1}^N W_{ij} (x_i - \bar{x})(x_j - \bar{x})}{\sum_{j=1}^N (x_i - \bar{x})^2} \quad (10)$$

where N is the number of spatial observation cells, x_i is the observed value of cell i , \bar{x} is the mean of x_i , $\bar{x} = \frac{1}{N} \sum_{i=1}^N x_i$, and $S_0 = \sum_{i=1}^N \sum_{j=1}^N W_{ij}$. W_{ij} is the spatial weighting value between the cell i and j , indicating the influence extent of spatial structure dependence, and determined according to adjacent relationship in this paper. After the Global Moran's I statistic of the LST is computed, its normalized Z-Score calculated by the Eq. 11 is used for statistical test of the result:

$$z(I) = \frac{I - E(I)}{S(I)} \quad (11)$$

where $E(I)$ and $S(I)$ are the mean and standard deviation of the Global Moran's I , respectively. To determine if the Z-Score is statistically significant, we can compare it to the range of values for a particular confidence level. For example, at a significance level of 0.05, a Z-Score would have to be less than -1.96 or greater than 1.96 to be statistically significant.

The value of Global Moran's I ranges from -1 to 1 . Given a certain significance level, a Moran's I value significantly beyond zero implies spatial positive correlation and obvious spatial clusters of cells with higher attribute values or lower attribute values, and the Moran's I near $+1.0$ indicates a small global spatial difference. On the other hand, a Moran's I value significantly below zero implies spatial negative correlation and an obvious spatial difference in the attribute values between the cells and their adjacent cells, and the Moran's I near -1.0 indicates a large global spatial difference. While a Moran's I value near $-1/(N - 1)$ indicates the pattern expressed is spatially random without spatial autocorrelation.

To explore the spatial autocorrelation of the LST field in the study area at different scales, the resultant LST images are resampled to the spatial resolution of 180, 540 and 1,080 m. At different levels of spatial resolution, the values of Global Moran's I of the LST images in 2002 are all significantly positive, which indicates that the LST field in Shanghai central city has a characteristic of spatial aggregation with significant spatial positive correlation. The distribution pattern of LST field shown in Figs. 2, 3 also confirms the existence of this spatial aggregation pattern. The value of Global Moran's I decreases as the spatial scale increases, the Global Moran's I reaches 0.795, 0.651

and 0.367, and the normalized Z-score of Moran's I is 276.940, 73.355 and 15.193 at the scale of 180, 540 and 1,080 m, respectively, much greater than the test threshold of normal distribution function at the significance level of 0.05. It can be concluded that the LST values in the neighborhood show a certain similarity at a small spatial scale, while the difference of neighboring LST values sharply increases and the similarity minishes as the scale increases. To reveal the temporal change tendency of the overall distribution pattern of LST field in the study area, the computed Global Moran's I of the LST images with 180 m resolution in 1989, 1997 and 2000 are 0.857, 0.851 and 0.839, and their normalized Z-scores are 291.683, 288.259 and 284.689, respectively. These results show that, under the impact of human activity, the LST field in central city tends to fragmentize and complicate with the development of the city, its global spatial difference becomes greater gradually, and therefore, its spatial autocorrelation has a trend of decrease year by year.

4.2 Local spatial autocorrelation analysis of LST field

The Global Moran's I only indicates overall clustering extent but cannot be used to detect spatial association pattern in different locations. To further reveal the spatial autocorrelation of LST in neighborhood space and visualize the spatial pattern of local difference, the local spatial autocorrelation statistics, including Local Moran's I_i and Getis-Ord's G_i^* are used to evaluate the local spatial association and difference between each cell and its surrounding cells.

4.2.1 Local Moran's I statistic

The Local Indicators of Spatial Association (LISA), such as Local Moran's I and Local Geary's C can be adopted to measure the spatial difference in the attribute values between each cell and its surrounding cells and its significance. Local Moran's I is the disintegration form of Global Moran's I . For a given spatial cell i , the value of Local Moran's I is computed as (Anselin 1995):

$$I_i = x_i \sum_{j=1, j \neq i}^N w_{ij} x_j \quad (12)$$

where N is the number of spatial observation cells, x_i and x_j are the standardized observed value of cell i and j , and w_{ij} is the standardized spatial weighting value, $\sum_j w_{ij} = 1$. Similar to the significance test of Global Moran's I , the result of Local Moran's I can be tested by means of Z-Score.

Given a certain significance level, if the I_i value is significantly positive, then the cell i has value similar to

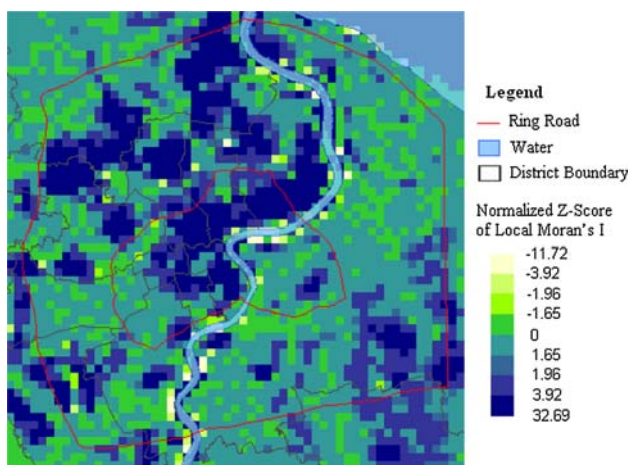


Fig. 4 Distribution of normalized Z-Score of Local Moran's *I* of LST field in 2002

neighboring cells' values, and a spatial cluster of similar LST values surrounds the cell *i*, which indicates a spatial positive correlation. A high positive *I_i* value demonstrates a strong clustering extent. On the other hand, if the *I_i* value is significantly negative, then the cell *i* has a very different LST value than its neighbors, which indicates a spatial negative correlation.

The distribution of normalized Z-Score of Local Moran's *I* of LST field with 540 m resolution in central city in 2002 is shown in Fig. 4. It can be found from the figure that the regions having significant spatial positive correlation with Z-Score beyond 1.65 are mainly distributed along the west bank of Hangpu River and the banks of Suzhou River, over the Wusong industrial zone in the northern area, Zhabei industrial zone, and the junction of Zhabei, Baoshan and Putuo, where are cluster zones of high LST values, and besides, at the junction of southeastern Pudong, Nanhui and the out ring road, where are cluster zones of low LST values. These regions constituting the hot and cold spots in the distribution of LST field in central city have a typical feature of small inner difference and large difference from outer regions. In addition, the cluster zones of high LST values are also located at the southern Putuo, northeastern Changning, and the junction of Minhang and Xuhui. On the other hand, the regions with Z-Score below -1.65 are mainly distributed near the banks of Hangpu River and the edges of cluster zones of high LST values, where are the transition zones of a mixture of high and low LST values in LST field with a typical feature of large inner difference and large difference from outer regions as well. The rests with Z-Score between -1.65 and 1.65 have no significant local spatial correlation.

4.2.2 Getis-Ord *G** statistic

To further evaluate the clustering extent and correlation of spatial distribution of attribute value in local regions, Getis and Ord (1992) proposed the *G** statistical method to identify the presence of clusters of extremely high or low values and determine spatial clustering pattern by presetting a certain spatial scale. Suppose there is an *n*-pixel image, the Getis-Ord *G_i^{*}* statistic is defined as the ratio of the sum of the weighted attribute values of the pixels within a specified distance *d* of a particular observation pixel *i* (including the pixel *i*) to the sum of the values of all *n* pixels in the entire image:

$$G_i^*(d) = \frac{\sum_{j=1}^n W_{ij}(d)x_j}{\sum_{j=1}^n x_j} \tag{13}$$

where *W_{ij}(d)* is the spatial weighting value, the pixels with nonzero *W_{ij}* constitute a computation window centred on the *i*th pixel. The shape of the window is defined according to the study aim and image characteristics. If a square window is used, then *W_{ij}(d)* is set to 1 as the *j*th pixel is within the distance *d* of the *i*th pixel, otherwise it is set to zero. The spatial scale *d* can be usually set to 1 (3 × 3 pixels window), 2 (5 × 5 pixels window), or 3 (7 × 7 pixels window).

The normalized Z-Score of *G_i^{*}(d)* is calculated as

$$Z_i(d) = \frac{G_i^*(d) - E(G_i^*(d))}{\sqrt{Var(G_i^*(d))}} = \frac{\sum_j W_{ij}(d)x_j - W_i^*\bar{x}}{s[W_i^*(n - W_j^*)/(n - 1)]^{1/2}} \tag{14}$$

where *W_i^{*}* = $\sum_{j=1}^n W_{ij}(d)$, \bar{x} = $\sum_{j=1}^n x_j/n$, and s^2 = $\sum_{j=1}^n x_j^2/n - \bar{x}^2$. A significant positive *Z_i(d)* value indicates spatial pattern of clustering of high values, that is, the cell *i* is surrounded by high attribute values. The higher the *Z_i(d)* value, the stronger the association. On the other hand, a significant negative *Z_i(d)* value indicates spatial pattern of clustering of low values, that is, the neighbors of cell *i* have low attribute values. Therefore, Getis-Ord *G** statistics can be used to identify spatial clusters of statistically significant high or low attribute values. A *Z_i(d)* near 0 indicates no apparent concentration and the neighbors have a range of values.

To clearly illustrate the spatial clustering pattern of LST field in the study area, and make a comparison with the result of Local Moran's *I*, the normalized Z-Score of *G_i^{*}* statistic is calculated at the scale *d* = 1. Figure 5 shows the distribution of normalized Z-Score of *G_i^{*}* of LST field with 540 m resolution in central city in 1997 and 2002, where navy blue represents cluster zones of high LST value, and light green represents cluster zones of low LST value. It can be found from the figure that the cluster zones of high

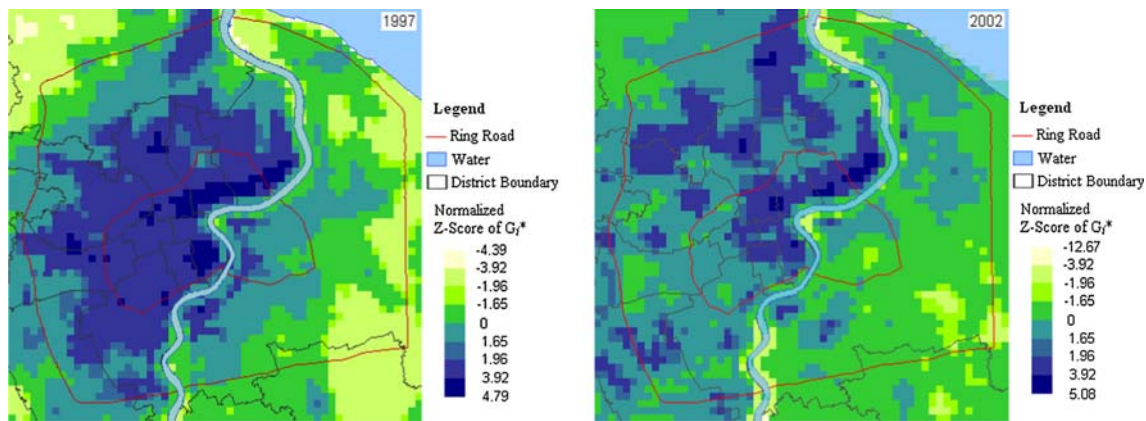


Fig. 5 Distribution of normalized Z-Score of G_i^* of LST field in 1997 and 2002

and low LST values in LST field in Shanghai central city tend to shrink and fragmentize, and accordingly, the cluster centers come to scatter. In 1997, the cluster zones of high LST value with Z-Score beyond 1.96 spread over most districts in Puxi area inside the out ring road and the belt from Lujiazui to the steel work and glass work in Pudong area on the east bank of Huangpu River. And the cluster centers of high LST value occur in Shanghai old urban area covering Huangpu and southern part of Yangpu, Hongkou and Zhabei on the west bank of Huangpu River. On the other hand, the cluster zones of low LST value with Z-Score below -1.96 are mainly distributed over partial Baoshan outside the out ring road, partial Pudong near the out ring road, and the junction of the southeastern Pudong and Nanhui. In 2002, the cluster zones of high and low LST values both shrink markedly. The cluster zones of high LST are divided into three regions, which are Shanghai old urban area on the west bank of Huangpu River, Zhabei industrial zone and its junction with Baoshan and Putuo, and the belt from Wusong industrial zone in Baoshan to the northwestern Yangpu. The cluster zones of low LST are only located at the southeastern area near the out ring road, and the northern and southern ends of Huangpu River in the study area. In addition, by comparison between Figs. 2 and 5, it can be found that, some high LST centers in LST field in Fig. 2 do not correspond to the centers of high Z-Score in Fig. 5, because these LST centers have a lower spatial correlation, meanwhile, some pixels having not extremely high LST but surrounded by high LST appear in the high Z-Score zones.

The above analyses indicate that, based on the comparison and calculation of the adjacent observed values, the G^* statistical method will not be affected by different acquisition times of remote sensing images and uncertainty in observation process, so it can be applied to explore the spatial pattern and temporal evolution of LST field in Shanghai central city effectively. Since 1990s, an amount

of population and industrial area in the downtown has been evacuating and moving out, the cluster zones of high LST inside the inner ring road gradually shrink. As the city further expands, the formation of new industrial and population aggregation areas not only results in the occurrence of new high LST clusters, but the shrink and even disappearance of original low LST clusters as well. Besides, in comparison with the result of Local Moran's I , Getis-Ord G^* statistics cannot detect the regions of spatial negative correlation, while it can precisely locate spatial cluster zones and centers, differentiate high LST clusters from low ones. The cluster area identified by G^* statistics is smaller than Local Moran's I , however, it is more consistent with the real spatial pattern of LST field.

4.3 Spatio-temporal variation characteristics of LST field

As a powerful tool for spatial heterogeneity exploration, geostatistical methods, combined with GIS, can help us to discover the inherent structure characteristics and spatial variation regularity of spatial variable which cannot be found by classical statistical method. Influenced by various natural and human factors, urban surface thermal landscape will present highly spatial heterogeneity. In this paper, geostatistical methods are adopted to qualitatively describe the characteristics of spatio-temporal variation of LST field in Shanghai central city. Based on the results of geostatistical analysis, the dynamic change of LST field is spatially interpolated by Kriging method.

The semivariogram, $\gamma(h)$, measures the difference in the attribute value between two random samples at all separation distances, and is defined as the variance of the difference (Journel and Huijbregts 1978; Olea 2006):

$$\gamma(h) = \frac{1}{2N(h)} \sum_{i=1}^{N(h)} [Z(x_i) - Z(x_i + h)]^2 \quad (15)$$

where h is the spatial separation distance of two samples, $Z(x_i)$ and $Z(x_i + h)$ are the observed values of the regionalized variable $Z(x)$ at the two locations x_i and $x_i + h$ ($i = 1, 2, \dots, N(h)$), $N(h)$ is the total number of the pairs of samples at the separation distance h .

Affected by various external factors, the level of spatial heterogeneity may be dissimilar in different directions. So the semivariogram changes not only with distance but also with direction (Cressie 1991; Journel and Huijbregts 1978). This is called anisotropy, which is described for the anisotropic semivariogram, denoted by $\gamma(h, \theta)$. The anisotropic ratio $K(h)$ can be used to describe the characteristic of anisotropic structure, and it is calculated as

$$K(h) = \gamma(h, \theta_1) / \gamma(h, \theta_2) \tag{16}$$

where $\gamma(h, \theta_1)$ and $\gamma(h, \theta_2)$ are the semivariograms at the direction θ_1 and θ_2 , respectively. A $K(h)$ near 1 indicates that the spatial heterogeneity is isotropic, otherwise, anisotropic.

Semivariogram is a general indicator to quantify the spatial dependence and heterogeneity of geographical distribution. The essential statistic parameters of semivariogram including nugget (C_0), partial sill (C), sill ($C_0 + C$), range (A_0), ratio of nugget to sill ($C_0 / (C + C_0)$) and anisotropic ratio (K) are used to discover the spatial heterogeneity characteristic of dynamic change of LST field in Shanghai central city. In the semivariogram, the nugget C_0 is comprised of measurement error and microscale variation, i.e., a random part of spatial heterogeneity, the partial sill C represents the spatial heterogeneity arising from spatial autocorrelation, and the sill $C_0 + C$ represents the total extent of spatial heterogeneity of the system property. Therefore, the ratio of nugget to sill $C_0 / (C_0 + C)$ indicates the proportion of the spatial heterogeneity arising from random factors in the total spatial heterogeneity, while

$C / (C_0 + C)$ indicates the contribution of structural factors to the total spatial heterogeneity. Range A_0 is the upper limit of distance within which the spatial correlation exists among sample data, and at A_0 the semivariogram levels off to the sill.

To illustrate the spatial variation pattern of the dynamic change of LST field in the study area, the difference of LST value with 180 m resolution in 2002 and 1997 is used as sample data, and the resulted isotropic and anisotropic semivariograms and their theoretical models for LST field changes from 1997 to 2002 are shown in Figs. 6 and 7 and Table 2. In the isotropic analysis, the semivariogram can be fitted by Gaussian model, in which the sill $C_0 + C$ is 5.975, and the ratio of nugget to sill $C_0 / (C + C_0)$ is 0.387, indicating a moderate spatial autocorrelation. On the other hand, the results of anisotropic computation in the direction of 0, 45, 90 and 135° show that the theoretical semivariograms in all directions are fitted for exponential model, in which the anisotropic ratio K is 1.396, indicating that the directional difference of dynamic change of LST field exists but is not obvious. So we cannot determine the major axial direction of the change of LST field in the study area at macroscale. Although the spatial distribution of LST

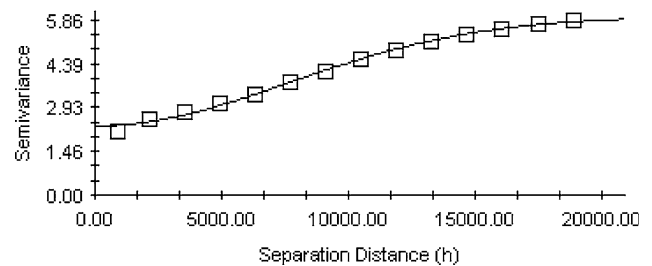


Fig. 6 Isotropic semivariogram of dynamic change of LST field from 1997 to 2002

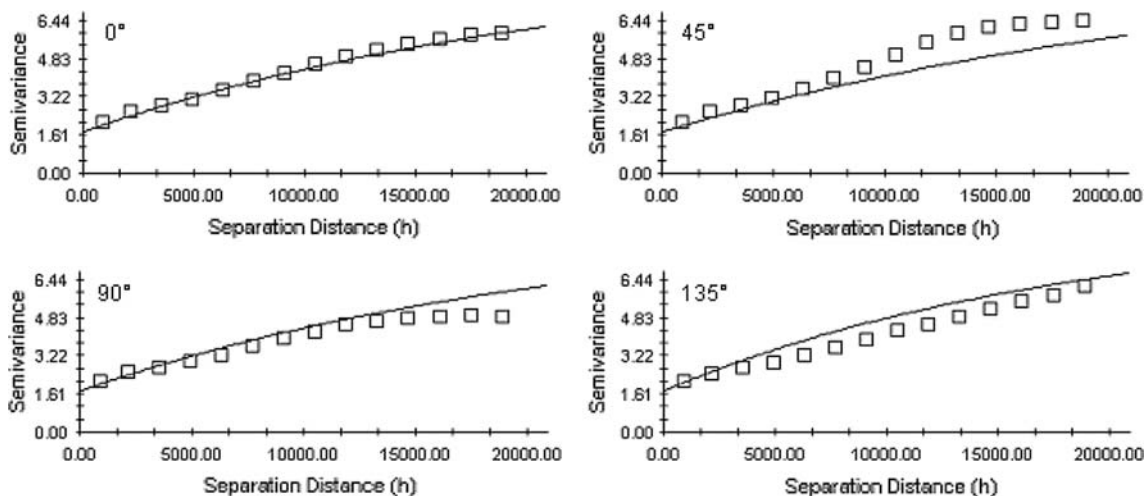
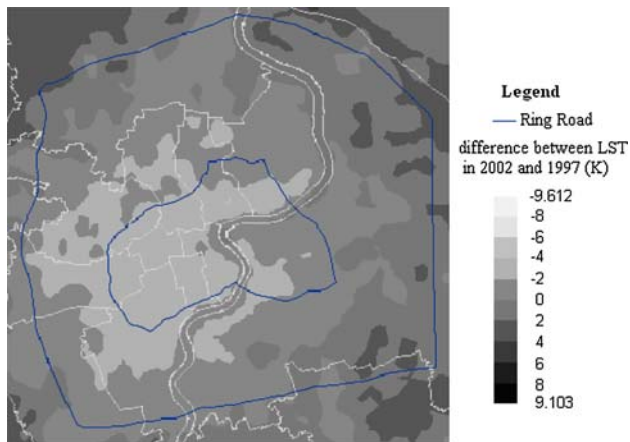


Fig. 7 Anisotropic semivariograms of dynamic change of LST field from 1997 to 2002

Table 2 Theoretical semivariograms and parameters of dynamic change of LST field from 1997 to 2002

	Model	C_0	$C_0 + C$	$C_0/(C_0 + C)$	A_0 (m)	K	r^2	RSS	
Isotropic	Gaussian model	2.310	5.975	0.387	10770	/	0.997	0.069	
Anisotropic	Exponential model	1.725	8.995	0.192	A_{major} 25360	A_{mirror} 18170	1.396	0.986	4.730

**Fig. 8** Kriging map of temporal change of LST field from 1997 to 2002

field will represent a local directional characteristic along with the change of various human and natural factors, the city of Shanghai expands in a circular pattern as a whole, the directional extent of dynamic change of urban surface thermal landscape is not very evident. The ratio of nugget to sill $C_0/(C + C_0)$ is 0.192 in all directions, indicating that the spatial heterogeneity arising from spatial autocorrelation is the main part of the total heterogeneity, and the extrema of temporal change in LST field have a characteristic of spatial clustering.

Based on the resultant theoretical models and parameters of the semivariogram, the differences between the LST in 2002 and 1997 are interpolated by Kriging method, and the spatial continuous surface of dynamic change of LST field is obtained. From the Kriging map shown in Fig. 8, it can be found that the dynamic change of LST field in the study area from 1997 to 2002 presents a tendency of increase in circularity. The LST difference transits gradually from negative value inside the central city to positive value outside the central city, and the critical profile of zero is located at the inner side of the out ring road. Although the utilized remote sensing images in the two years have seasonal difference, it still can be concluded that LST declines distinctly in the Puxi and Pudong area near and inside the inner ring road, which covers the south of Yangpu and Hongkou, the middle and south of Zhabei and Putuo, the east of Changning, the middle and north of Xuhui, Jing'an, Luwan, Huangpu, and the south of Pudong

along the Huangpu River. On the other hand, LST rises evidently near the out ring road and outside the central city, mainly distributed over Baoshan to the north of the out ring road, and Pudong and Nanhui near the out ring road.

5 Conclusions

In this paper, based on the LST retrieval from Landsat TM6 and ETM + 6 data of Shanghai central city in 1989, 1997, 2000 and 2002, ESDA is applied to quantify the characteristics of spatial heterogeneity and temporal evolution of land surface thermal landscape at different scales and periods in Shanghai central city, by utilizing global and local spatial autocorrelation analysis and geostatistical methods. The spatial variance pattern of the change of LST field from 1997 to 2002 indicates that the extrema of temporal change in LST field have a characteristic of spatial clustering. As the city of Shanghai expands in a circular pattern as a whole, the directional difference of dynamic change of urban surface thermal landscape exists but is not obvious. Besides, it can be found from the Kriging map of the LST difference during the study period, that the dynamic change of LST in the study area exhibits a tendency of increase in circularity, that is, LST difference transits gradually from negative value inside the central city to positive value outside the central city, and the critical profile of zero is located at the inner side of the out ring road. LST declines distinctly in the Puxi and Pudong area near and inside the inner ring road, while it rises near the out ring road and outside the central city. Future research will focus on monitoring and studying urban heat island at multiple spatial and temporal scales by comprehensively utilizing remote sensing images with different spatio-temporal and spectral resolutions.

Acknowledgments The work described in this paper was funded by National Key Fundamental Research and Development Program (2008DFB90240 and 200805080) and Project of key course for graduate student of East China Normal University (2007kc04). The authors also appreciate the editors and reviewers for their constructive comments and suggestions on our paper.

References

- Anselin L (1995) Local indicators of spatial association—LISA. *Geogr Anal* 27:93–115

- Anselin L (1999) Interactive techniques and exploratory spatial data analysis. In: Longley PA, Goodchild MF, Maguire DJ (eds) *Geographical information systems: principles, technical issues, management issues and applications*. Wiley, New York, pp 253–266
- Brenning A, Dubois G (2008) Towards generic real-time mapping algorithms for environmental monitoring and emergency detection. *Stoch Environ Res Risk Assess* 22:601–611
- Chander G, Markham B (2003) Revised Landsat 5 TM radiometric calibration procedures and post-calibration dynamic ranges. *IEEE Trans Geosci Remote Sens* 41:2674–2677
- Chen Y, Shi P, Li X, He C (2002) Research on urban spatial thermal environment using remote sensing image. *Acta Geodaetica et Cartographica Sinica* 31:322–326
- Cressie NAC (1991) *Statistics for spatial data*. Wiley, New York
- Dai X, Guo Z, Zhang L, Wu J (2009) Spatio-temporal pattern of urban land cover evolution with urban renewal and expansion in Shanghai based on mixed-pixel classification for remote sensing imagery. *Int J Remote Sens* (accepted)
- Ding F, Xu H (2006) Comparison of two new algorithms for retrieving land surface temperature from Landsat TM thermal band. *Geo-Inform Sci* 8:125–130
- Gallo KP, Tarpley JD, McNab AL (1995) Assessment of urban heat islands: a satellite perspective. *Atmospheric Res* 37:37–43
- Getis A, Ord JK (1992) The analysis of spatial association by use of distance statistics. *Geogr Anal* 24:189–206
- Goodchild (1986) *Spatial autocorrelation (CATMOG47)*. Geobooks, Norwich, UK
- Huang M, Xing X, Wang P (2006) Comparison between three different methods of retrieving surface temperature from Landsat TM thermal infrared band. *Arid Land Geogr* 29:132–137
- Janssen M (1998) *Modeling global change—the art of integrated assessment modeling*. Elgar, Edward
- Journel AG, Huijbregts CJ (1978) *Mining geostatistics*. Academic Press, New York
- Keller CF (2008) Global warming: a review of this mostly settled issue. *Stoch Environ Res Risk Assess*. doi:[10.1007/s00477-008-0253-3](https://doi.org/10.1007/s00477-008-0253-3)
- Ma R, Huang X, Zhu C (2002) Knowledge discovery with ESDA from GIS database. *J Remote Sens* 6:102–106
- Morakinyo JA, Mackay R (2005) Geostatistical modelling of ground conditions to support the assessment of site contamination. *Stoch Environ Res Risk Assess* 20:106–118
- Olea RA (2006) A six-step practical approach to semivariogram modeling. *Stoch Environ Res Risk Assess* 20:307–318
- Owen TW, Carlson TN, Gillies RR (1998) An assessment of satellite remotely-sensed land cover parameters in quantitatively describing the climatic effect of urbanization. *Int J Remote Sens* 19:1663–1681
- Qin Z, Kanieli A, Berliner P (2001) A mono-window algorithm for retrieving land surface temperature from Landsat TM data and its application to the Israel-Egypt border region. *Int J Remote Sens* 22:3719–3746
- Qin Z, Li W, Xu B (2004) Estimation method of land surface emissivity for retrieving land surface temperature from Landsat TM6 data. *Adv Mar Sci* 22:129–137
- Snyder WC, Wan Z, Zhang Y, Feng YZ (1998) Classification-based emissivity for land surface temperature measurement from space. *Int J Remote Sens* 19:2753–2774
- Streutker DR (2002) A remote sensing study of the urban heat island of Houston, Texas. *Int J Remote Sens* 23:2595–2608
- Tamerius JD, Wise EK, Uejio CK, McCoy AL, Comrie AC (2007) Climate and human health: synthesizing environmental complexity and uncertainty. *Stoch Environ Res Risk Assess* 21:601–613
- Tran H, Daisuke U, Shiro O, Yoshifumi Y (2006) Assessment with satellite data of the urban heat island effects in Asian mega cities. *Int J Appl Earth Obs Geoinform* 8:34–48
- Wan Z, Dozier JA (1996) Generalized split-window algorithm for retrieving land-surface temperature from space. *IEEE Trans Geosci Remote Sens* 34:892–905
- Wukelic GE, Gibbons DE, Martucci LM, Foote HP (1989) Radiometric calibration of Landsat Thematic Mapper Thermal Band. *Remote Sens Environ* 28:339–347
- Xu H, Chen B (2003) An image processing technique for the study of urban heat island changes using different seasonal remote sensing data. *Remote Sens Tech Appl* 18:129–133
- Zhang Z, He G, Xiao R (2005) A study on the new algorithms for retrieving land surface temperature based on TM6 data. *Remote Sens Technol Appl* 20:547–550
- Zhang J, Wang Y, Wang Z (2007) Change analysis of land surface temperature based on robust statistics in the estuarine area of Pearl River (China) from 1990 to 2000 by Landsat TM/ETM + Data. *Int J Remote Sens* 28:2383–2390